Journal of Engineering Mathematics 20 (1986) 233–250


# Fluid flow in a partially-filled rotating cylinder

G.J.F. VAN HEIJST

*University of Utrecht, Institute of Meteorology and Oceanography, Princetonplein 5, Utrecht, The Netherlands*

(Received April 7, 1986)

**Summary.**

This paper presents an analytical description of the fluid flow in a partially-filled cylinder rotating at a sufficiently high rate that the fluid forms a film of uniform thickness against the sidewall. Relative flow is induced by differential rotation of the upper endcap of the cylinder. When the film thickness is large enough, the main body of the fluid is in geostrophic balance, viscous effects being confined within thin shear layers at the flow boundaries. At the horizontal endcaps these layers are of Ekman type, while Stewartson layers arise at the sidewall and at the free surface. In contrast with the Stewartson layer at the sidewall, which has a sandwich structure consisting of layers of thicknesses $E^{1/4}$ and $E^{1/3}$, viscous effects at the free surface are concentrated in a single layer of thickness $E^{1/3}$ ($E$ is the Ekman number). The theoretical velocity profiles are compared with numerical and experimental profiles presented by Shadday, Ribando and Kauzlarich [1] and the agreement is very good. The comparison is also made in the thin-film situation where the Stewartson layers partially overlap, and again the theoretical profiles agree fairly well with the numerical and experimental results.

## 1. Introduction

The relative fluid flow in a rapidly rotating cylinder has attracted many investigators, and a large number of studies on the subject have appeared. Due to their relevance to geophysical and engineering problems, rotating fluids have been studied in a variety of configurations, ranging from wind-driven ocean models to models of gas centrifuges as used for the enrichment of natural uranium.

Under certain conditions the main body of a contained rotating fluid can be in geostrophic balance, with viscous effects being confined within thin layers at the solid boundaries. The shear layers arising at the horizontal flow boundaries are called Ekman layers, which may also occur at a free upper surface if shear is exerted there. Another type of shear layer arising in a contained rotating fluid is the so-called Stewartson layer; usually it is present at lateral boundaries of the flow (see e.g. Johnson [2], Conlisk and Walker [3,4], van Heijst [5]), but it may also occur as a detached layer induced by bottom topography, by moving objects, or by singularities on the horizontal boundaries, see e.g. Stewartson [6], Moore and Saffman [7], Hashimoto [8]. Stewartson layers generally have a sandwich structure consisting of an outer layer of thickness $E^{1/4}$ and an inner layer of thickness $E^{1/3}$, with $E$ the Ekman number of the flow.

Though the majority of studies on rotating shear layers were devoted to configurations of fluid in a completely filled container (with a solid lid as an upper boundary), a number

of investigators has examined the effect of a stress-free upper surface on the circulation in a partially-filled rotating cylinder. Shadday, Ribando and Kauzlarich [1] have recently investigated the flow in a partially-filled cylinder rotating at extremely high rate, such that all the fluid is confined in a film of approximately uniform thickness at the sidewall. Thus a *vertical* free surface arises, on which the shear stress vanishes. Weak relative fluid motion is induced by differential rotation of the upper endcap of the cylinder. Shadday et al. have carried out accurate velocity measurements by use of a laser-Doppler velocimeter and these results were compared with numerical calculations of the flow. The numerical model, based on the finite-difference technique, yielded solutions to the full nonlinear axisymmetric governing equations, and showed good agreement with the experimental results. From their work it appears that, in the case that the upper endcap rotates faster than the cylinder, the upper Ekman layer produces a radially-outward flow, which is forced downward along the cylinder sidewall via a Stewartson shear-layer. An Ekman layer at the bottom disk carries the fluid radially inwards, and, due to the differential Ekman suctions, a weak axial return flow occurs in the fluid interior. As the geostropic flow in axial direction is very weak, a significant portion of the axial return flow is concentrated in a thin Stewartson-type shear layer at the free surface.

The objective of the present paper is to examine this flow configuration analytically, i.e. by using the familiar perturbation technique generally applied in Stewartson-layer theory. This theoretical approach is thought to be useful because the results obtained by Shadday et al. [1] offer the opportunity to verify the accuracy of the "classical" Stewartson-layer analysis. Accurate velocity measurements in Stewartson layers are scarce, mainly due to serious restrictions posed by the small thickness of such shear layers in laboratory configurations. Until recently, velocity measurements in rotating shear layers were carried out by applying the thymol-blue technique described by Baker [9]. This visualization technique has been used to measure velocities in Stewartson's [6] split-disk configuration and, though the qualitative agreement between the theoretical and experimental profiles was satisfactory, the magnitude of the theoretical velocity was in some cases found to exceed the experimental value by about 30%, see Baker [10]. Some years later, Cook and Ludford [11] included curvature effects in the theoretical shear-layer analysis, and thus reduced the discrepancy between theory and experiment by about 7%. This improvement is still insufficient to explain the whole 30%-gap, and the remaining discrepancy was attributed to nonlinear effects.

Although the analysis in the present paper is essentially linear, the agreement with the numerical results obtained by Shadday et al. [1] is very good. Formally, the theoretical description only applies to the "thick-film case", in which the film thickness is large enough as that the Stewartson shear-layers at the sidewall and at the free surface are separated by a geostrophic interior region. Shadday et al. have also examined the "thin-film case", where the inviscid interior has vanished and the Stewartson layers merge; for this case a correction is needed in the shear-layer analysis, and it turns out that the theoretical results agree fairly well with the numerical calculations.

The experimental results obtained by Shadday et al. are generally in accordance with the numerical and analytical velocity profiles, though near the free surface some deviations occur both in the azimuthal and in the vertical velocity components (the observed magnitudes are lower than those calculated analytically or numerically). It is believed that the discrepancy has some instrumental origin, as the numerical and theoretical curves do correspond there.

## 2. Formulation

Consider the flow configuration as schematically depicted in Figure 1. Due to the high rotation rate $\Omega$ the fluid in the partially-filled rotating cylinder (radius $bL$, height $HL$) is concentrated in a thin film at the sidewall. The film thickness is assumed to be uniform, and measures $(b-a)L$. The upper endcap of the cylinder rotates slightly faster with angular velocity $(1+\epsilon)\Omega$, $0<\epsilon\ll 1$. In the following the fluid flow is related to a co-rotating cylindrical coordinate system $(r, \theta, z)$, with $z$ pointing in the axial direction; the corresponding velocity components in radial, azimuthal and axial direction are denoted by $(u, v, w)$. Lengths and velocities are non-dimensionalized by $L$ and $\epsilon\Omega L$, respectively. Assuming that the relative motion is small enough as to neglect nonlinear effects, the steady flow of an incompressible fluid relative to the rotating frame is governed by

$$2\mathbf{k}\times\mathbf{v} = -\nabla p + E\nabla^2\mathbf{v}, \tag{1a}$$

$$\nabla\cdot\mathbf{v} = 0, \tag{1b}$$

with $\mathbf{v}$ the velocity vector, $p$ the reduced pressure, and $\mathbf{k}=\boldsymbol{\Omega}/\Omega$ the unit vector in axial direction; $E$ is the Ekman number, defined as $E=\nu/\Omega L^2$, $\nu$ being the kinematic fluid viscosity. The objective of the subsequent analysis is to provide a solution to (1) in the region $a\leqslant r\leqslant b$, $0\leqslant z\leqslant H$ under the conditions

$$\begin{aligned}&\mathbf{v}=(0,0,0) \quad \text{at} \quad (z=0,\ a\leqslant r\leqslant b) \quad \text{and} \quad (0\leqslant z<H,\ r=b),\\ &\mathbf{v}=(0,r,0) \quad \text{at} \quad (z=H,\ a\leqslant r<b),\end{aligned} \tag{2}$$

and vanishing shear stress at the free surface ($r=a$, $0<z<H$).

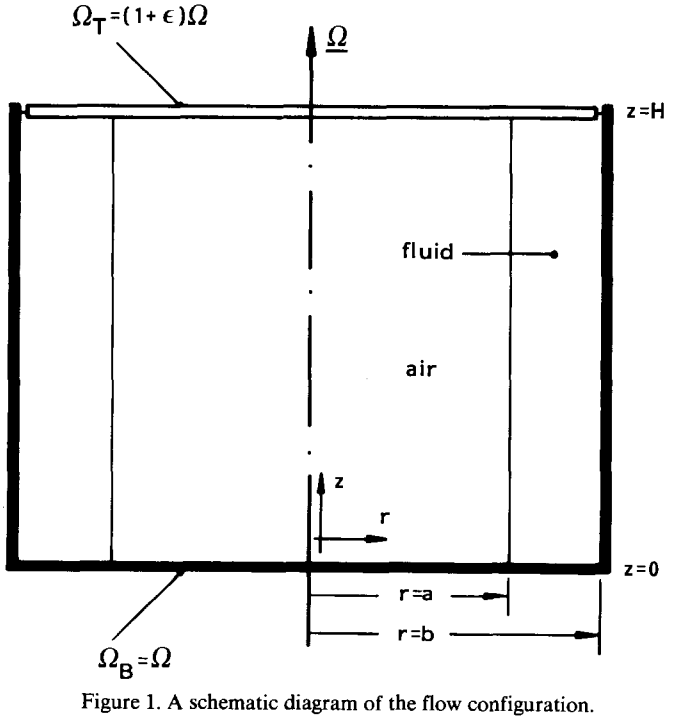


Figure 1. A schematic diagram of the flow configuration.

When the film thickness is large enough, the flow at some distance from the solid boundaries is in geostrophic balance, and is governed by the Ekman layers at the horizontal endcaps ($z = 0,\ H$). By use of the well-known Ekman suction conditions one derives

$$u_I = 0, \quad v_I = \tfrac{1}{2}r, \quad w_I = \tfrac{1}{2}E^{1/2}, \tag{3}$$

where the subscript $I$ refers to the interior. The geostrophic motion is apparently one of a solid-body rotation plus a weak axial flow $O(E^{1/2})$ towards the faster rotating endcap. At the horizontal boundaries the Ekman layers carry radial $O(E^{1/2})$ transports $Q$ of magnitude

$$Q(z = 0) = -\tfrac{1}{4}rE^{1/2}, \quad Q(z = H) = +\tfrac{1}{4}rE^{1/2}. \tag{4}$$

It is now clear that the Stewartson layer at the cylinder sidewall ($r = b$) has a double task in providing a smooth transition to zero for the interior swirl velocity and besides producing an $O(E^{1/2})$ transport from the upper to the lower Ekman layer. Axial return flow $O(E^{1/2})$ takes place in the geostrophic interior, but as this is not sufficient, another Stewartson layer arises at the free surface ($r = a$) in order to provide an additional vertical $O(E^{1/2})$ flux.

## 3. The thick-film case

In this case it is assumed that the thicknesses of the Stewartson shear layers at the free surface and at the sidewall are small compared to the film thickness, so that the shear layers are separated by a non-viscous interior flow region.

### *3.1. The boundary layer at the sidewall*

The shear layer at the cylinder wall is of Stewartson type, and has a sandwich structure consisting of two layers of thicknesses $E^{1/4}$ and $E^{1/3}$. The thicker $E^{1/4}$ layer usually provides the matching of O(1) velocities and produces some vertical $O(E^{1/2})$ transport, while the essential task of the $E^{1/3}$ layer lies in performing the higher-order matching and in completing the vertical $O(E^{1/2})$ flux. As their structure has extensively been examined in previous studies (see e.g. [2,5,6,7,13]), the present discussion of the Stewartson $E^{1/4}$ and $E^{1/3}$ layers will be brief.

#### *3.1.1. The $E^{1/4}$ layer*

The velocity components and the pressure in the $E^{1/4}$ layer are expanded as

$$(u,\ v,\ w,\ p) = \sum_{j=0}^{\infty} (E^{1/2}U^{(j)},\ V^{(j)},\ E^{1/4}W^{(j)},\ E^{1/4}P^{(j)})E^{j/4}, \tag{5}$$

and substitution into (1) yields, after elimination of the pressure:

$$U_z^{(0,1)} = V_z^{(0,1)} = W_{zz}^{(0,1)} = 0, \tag{6a}$$

$$V_{\xi\xi\xi}^{(0)} + 2W_z^{(0)} = 0, \tag{6b}$$

$$V_{\xi\xi\xi}^{(1)} + \frac{2}{b} V_{\xi\xi}^{(0)} + 2W_z^{(1)} = 0, \tag{6c}$$

$$2U^{(0,1)} = V_{\xi\xi}^{(0,1)}, \tag{6d}$$

where $\xi = (r-b)E^{-1/4}$ is the stretched radial coordinate. The Ekman layers at the endcaps impose the following suction conditions

$$W^{(0)} = \pm \tfrac{1}{2} V_\xi^{(0)}, \quad W^{(1)} = \pm \frac{1}{2}\left(\frac{1}{b} V^{(0)} + V_\xi^{(1)}\right) + \left(\tfrac{1}{2} \mp \tfrac{1}{2}\right), \quad z = \left(\tfrac{1}{2} \mp \tfrac{1}{2}\right) H. \tag{7}$$

By use of these, one derives from (6) an equation for $V^{(0)}$:

$$V_{\xi\xi\xi}^{(0)} - \frac{2}{H} V_\xi^{(0)} = 0, \tag{8}$$

the solution of which should satisfy the matching requirements $V^{(0)}(\xi \to -\infty) = v_I(b)$ and $V^{(0)}(\xi = 0) = 0$. For the leading-order terms ($j = 0$) one finds

$$\begin{aligned} V^{(0)}(\xi) &= \tfrac{1}{2} b\left[1 - \exp(s\xi)\right], \\ W^{(0)}(\xi, z) &= -\tfrac{1}{2} bs\left(\frac{1}{2} - \frac{z}{H}\right) \exp(s\xi), \\ U^{(0)}(\xi) &= -\frac{b}{2H} \exp(s\xi), \end{aligned} \tag{9}$$

with $s = \sqrt{2/H}$. The $V^{(0)}$ solution shows a correct adjustment to relative rest at the sidewall, but $U^{(0)}$ and $W^{(0)}$ do not satisfy the condition of no-slip at $\xi = 0$, which necessitates the presence of the $E^{1/3}$ layer to carry out the higher-order matching (this will be discussed later).

Similarly, one derives for the next-order azimuthal velocity

$$V_{\xi\xi\xi}^{(1)} - \frac{2}{H} V_\xi^{(1)} = \frac{2}{b}\left(\frac{1}{H} V^{(0)} - V_{\xi\xi}^{(0)}\right) - \frac{2}{H}, \tag{10}$$

which has the following general solution

$$V^{(1)}(\xi) = A + B \exp(s\xi) + \tfrac{1}{4}\xi \exp(s\xi) + \tfrac{1}{2}\xi. \tag{11}$$

The constants $A$ and $B$ are determined by matching to the interior ($\xi \to -\infty$) and to the inner $E^{1/3}$ layer at $\xi = 0$. In the limit $r \to b$ the interior swirl velocity is

$$v_I(r \to b) = v_I(b) + E^{1/4} \xi \left.\frac{\partial v_I}{\partial r}\right|_b + \mathrm{O}(E^{1/2}), \tag{12}$$

and should match smoothly to the composite $E^{1/4}$-layer velocity

$$V(\xi \to -\infty) = V^{(0)}(\xi \to -\infty) + E^{1/4}V^{(1)}(\xi \to -\infty) + \mathrm{O}(E^{1/2})$$
$$= \tfrac{1}{2}b + \left(A + \tfrac{1}{2}\xi\right)E^{1/4} + \mathrm{O}(E^{1/2}). \tag{13}$$

This obviously requires $A = 0$. From the $E^{1/3}$-layer analysis it appears that the matching of the $\mathrm{O}(E^{1/4})$ swirl velocities in the outer and the inner layer demands $V^{(1)}(\xi = 0) = 0$, and therefore $B = 0$. The solution for $V^{(1)}$ is completely determined then, and that for $W^{(1)}$ follows directly from (6c), yielding

$$V^{(1)}(\xi) = \tfrac{1}{2}\xi\left[1 + \tfrac{1}{2}\exp(s\xi)\right],$$
$$W^{(1)}(\xi, z) = \tfrac{1}{4}(s\xi - 1)\left(\frac{1}{2} - \frac{z}{H}\right)\exp(s\xi) + \tfrac{1}{2}. \tag{14}$$

As $W^{(1)}$ does not satisfy the no-slip condition at the sidewall ($\xi = 0$), the adjustment to zero has to be performed by the inner $E^{1/3}$ layer.

The vertical $\mathrm{O}(E^{1/2})$ transport carried by the $E^{1/4}$ layer is

$$T(z) = \int_{-\infty}^{0} W^{(0)}(\xi, z)\,\mathrm{d}\xi = -\frac{1}{2}\left(\frac{1}{2} - \frac{z}{H}\right)b, \tag{15}$$

and it is obvious that an additional flux contribution is needed from the $E^{1/3}$ layer, in order to produce a net downward transport of magnitude $\frac{1}{4}bE^{1/2}$, see (4), from the upper to the lower Ekman layer.

*3.1.2. The $E^{1/3}$ layer*

The $E^{1/3}$-layer quantities are expanded in powers of $E^{1/12}$ according to

$$(u, v, w, p) = \sum_{j=0}^{\infty}\left(E^{1/3}\tilde{u}_j, \tilde{v}_j, \tilde{w}_j, E^{1/3}\tilde{p}_j\right)E^{j/12}, \tag{16}$$

and for the terms up to $j = 7$ one derives by substitution of (16) into (1):

$$2\frac{\partial \tilde{v}_j}{\partial z} = \frac{\partial^3 \tilde{w}_j}{\partial \eta^3}, \quad 2\frac{\partial \tilde{w}_j}{\partial z} = -\frac{\partial^3 \tilde{v}_j}{\partial \eta^3} \tag{17}$$

and

$$2\tilde{u}_j = \frac{\partial^2 v_j}{\partial \eta^2}, \tag{18}$$

with $\eta = (r - a)E^{-1/3}$ the scaled radial coordinate.

As mentioned in the previous section, the $E^{1/3}$ layer must accomplish a matching of $U^{(0)}$, $W^{(0)}$, $V^{(1)}$ and $W^{(1)}$ to the cylinder sidewall, and besides it must produce a vertical $\mathrm{O}(E^{1/2})$ flux of magnitude

$$\tilde{T}(z) = -\frac{bz}{2H} \tag{19}$$

in order to close the transport of fluid from the upper to the lower Ekman layer. Inspection of (16) learns that this can be performed by the $j = 2, 3, 6$ fields of the layer; the $j = 0, 1, 4, 5$ fields play no role of importance and can be regarded as being absent.

The $j = 2$ field must both accomplish the $U^{(0)}$-matching and produce the required vertical transport (19). Analysis of the Ekman extensions of the $E^{1/3}$ layer yields the following suction conditions:

$$\begin{aligned} \tilde{w}_2 &= 0 \qquad (z = 0), \\ \tilde{w}_2 &= -b\delta(\eta) \quad (z = H), \end{aligned} \tag{20}$$

and the conditions with respect to $\eta$ are

$$\tilde{u}_2,\ \tilde{v}_2,\ \tilde{w}_2 \to 0, \quad (\eta \to -\infty), \tag{21a}$$

$$\left.\begin{aligned} \tilde{u}_2 &= -U^{(0)}(0) = -\tfrac{1}{2}b/H \\ \tilde{v}_2 &= \tilde{w}_2 = 0. \end{aligned}\right\} (\eta = 0). \tag{21b}$$

Solutions to (17), (18) satisfying these conditions can be found by standard techniques, giving

$$\begin{aligned} \tilde{w}_2(\eta, z) &= -\sum_{n=1}^{\infty} A_n \phi_1(\gamma_n; \eta) \sin \frac{n\pi z}{H}, \\ \tilde{v}_2(\eta, z) &= -\sum_{n=1}^{\infty} A_n \phi_1(\gamma_n; \eta) \cos \frac{n\pi z}{H}, \\ \tilde{u}_2(\eta, z) &= +\tfrac{1}{4}\sum_{n=1}^{\infty} A_n \gamma_n^2 \left[\phi_1(\gamma_n; \eta) + \sqrt{3}\,\phi_2(\gamma_n; \eta)\right] \cos \frac{n\pi z}{H} \end{aligned} \tag{22}$$

with

$$A_n = \frac{-4b}{H\sqrt{3}} \frac{(-1)^n}{\gamma_n^2}, \quad \gamma_n = (2n\pi/H)^{1/3}$$

and

$$\begin{aligned} \phi_1(\gamma_n; \eta) &= \mathrm{e}^{-1/2\gamma_n|\eta|} \sin \tfrac{1}{2}\gamma_n |\eta| \sqrt{3} \\ \phi_2(\gamma_n; \eta) &= \mathrm{e}^{-1/2\gamma_n|\eta|} \cos \tfrac{1}{2}\gamma_n \eta \sqrt{3}\,. \end{aligned} \tag{23}$$

It is easy to verify that integration of the vertical velocity over the layer thickness indeed yields a transport as given by (19).

The $j = 3$ field of the $E^{1/3}$ layer has to perform the matching of $W^{(0)}$ and $V^{(1)}$ to the

cylinder wall. The appropriate boundary conditions are therefore

$$\tilde{u}_3,\ \tilde{v}_3,\ \tilde{w}_3 \to 0 \quad (\eta \to -\infty), \tag{24a}$$

$$\left.\begin{aligned} &\tilde{u}_3 = 0 \\ &\tilde{v}_3 = -V^{(1)}(\xi = 0) \\ &\tilde{w}_3 = -W^{(0)}(\xi = 0) = \tfrac{1}{2}bs\left(\frac{1}{2} - \frac{z}{H}\right), \end{aligned}\right\} (\eta = 0) \tag{24b}$$

to be completed by the Ekman suction conditions, which take (in the absence of the $j = 1$ field) the following form:

$$\tilde{w}_3 = 0 \quad (z = 0,\ H). \tag{24c}$$

The higher-order swirl velocity $V^{(1)}(\xi = 0)$ in the $E^{1/4}$ layer is given by (11), with $A = 0$ and $B$ still unknown. Though details are not presented here, it follows from the matching analysis that $V^{(1)}$ must satisfy $V^{(1)}(\xi = 0) = 0$, which determines the $O(E^{1/4})$ swirl velocity in the $E^{1/4}$ layer. Again, solving the equations (17) and (18) with respect to the conditions (24) is a standard problem, yielding

$$\begin{aligned} \tilde{w}_3(\eta,\ z) &= \sum_{n=1}^{\infty} B_n\left(\phi_3 + \phi_2 - \phi_1\sqrt{3}\right) \sin\frac{n\pi z}{H}, \\ \tilde{v}_3(\eta,\ z) &= -\sum_{n=1}^{\infty} B_n\left(\phi_3 - \phi_2 + \phi_1\sqrt{3}\right) \cos\frac{n\pi z}{H}, \\ \tilde{u}_3(\eta,\ z) &= -\tfrac{1}{2}\sum_{n=1}^{\infty} B_n\gamma_n^2\left(\phi_3 - \phi_2 - \phi_1\sqrt{3}\right) \cos\frac{n\pi z}{H}, \end{aligned} \tag{25}$$

with

$$B_n = \frac{(-1)^n + 1}{4n\pi}bs, \quad \phi_3 = \phi_3(\gamma_n;\ \eta) = \exp(-\gamma_n|\eta|) \tag{26}$$

and $\phi_1$, $\phi_z$ being given by (23). Integration of $\tilde{w}_3$ over the layer thickness shows that there is no net vertical transport $O(E^{7/12})$ in the $E^{1/3}$ layer: the motion to this order is merely recirculatory.

The $j = 6$ field of the $E^{1/3}$ layer has to accomplish the matching of $W^{(1)}$, which is only $O(E^{1/2})$; though its contribution to the shear-layer structure seems of minor importance, the results of the $j = 6$ field analysis are mentioned here for reasons of consistency, as the vertical velocity in the $E^{1/4}$ layer is also calculated to $O(E^{1/2})$. The boundary conditions for this field are:

$$\tilde{u}_6,\ \tilde{v}_6,\ \tilde{w}_6 \to 0 \quad (\eta \to -\infty), \tag{27a}$$

$$\left.\begin{aligned} &\tilde{u}_6 = \tilde{v}_6 = 0 \\ &\tilde{w}_6 = -W^{(1)}(\xi = 0) = \frac{1}{4}\left(\frac{1}{2} - \frac{z}{H}\right) - \tfrac{1}{2} \end{aligned}\right\} (\eta = 0), \tag{27b}$$

$$\tilde{w}_6 = 0 \quad (z = 0,\ H). \tag{27c}$$

In view of the suction conditions (27c), the general $\tilde{w}_6$ solution is written as a Fourier sine-series, and by using the series properties (see e.g. Tolstov [12])

$$\sum_{n=1}^{\infty} \frac{1}{n} \sin \frac{n\pi z}{H} = \frac{\pi}{2}\left(1 - \frac{z}{H}\right), \quad \sum_{n=1}^{\infty} \frac{(-1)^n}{n} \sin \frac{n\pi z}{H} = -\frac{\pi z}{2H}, \tag{28}$$

the matching condition for $\tilde{w}_6$ can be formulated as

$$\tilde{w}_6(\eta = 0) = -\sum_{n=1}^{\infty} \frac{3 - 5(-1)^n}{4n\pi} \sin \frac{n\pi z}{H}. \tag{29}$$

The solutions for $\tilde{w}_6$ and $\tilde{v}_6$ are then easily found to be

$$\begin{aligned} \tilde{w}_6(\eta, z) &= \sum_{n=1}^{\infty} C_n\left(\phi_3 + \phi_2 - \phi_1\sqrt{3}\right) \sin \frac{n\pi z}{H}, \\ \tilde{v}_6(\eta, z) &= \sum_{n=1}^{\infty} C_n\left(-\phi_3 + \phi_2 - \phi_1\sqrt{3}\right) \cos \frac{n\pi z}{H}, \end{aligned} \tag{30}$$

with

$$C_n = -\left[3 - 5(-1)^n\right]/8n\pi$$

and $\phi_1$, $\phi_2$, $\phi_3$ given by (23) and (26).

This completes the analysis of the Stewartson layer at the sidewall: the azimuthal and vertical velocity components in the shear layer have been determined to $O(E^{1/4})$ and $O(E^{1/2})$ accuracy, respectively.

### *3.2. The boundary layer at the free surface*

As pointed out in Section 2, the shear layer occurring at the free surface ($r = a$) must accomplish a return flow $O(E^{1/2})$ from the lower to the upper Ekman layer. The free surface allows the occurrence of non-zero azimuthal and vertical velocities, and therefore no O(1) matching is required like at solid boundaries. For this reason the $E^{1/4}$ layer is absent here, and the return flow must be entirely produced by the $j = 2$ field of the $E^{1/3}$ layer.

With regard to the analysis of the $E^{1/3}$ layer at $r = a$ it is useful to define the stretched radial coordinate as $\eta = (r - a)E^{-1/3}$, which is positive as $r \geqslant a$. The dynamical $E^{1/3}$-layer quantities are scaled as in (16), and are governed by the equations (17) and (18).

The boundary conditions for the $j = 2$ field are

$$\tilde{u}_2, \tilde{v}_2, \tilde{w}_2 \to 0 \qquad (n \to +\infty), \tag{31a}$$

$$\tilde{u}_2 = 0, \frac{\partial \tilde{v}_2}{\partial \eta} = 0, \frac{\partial \tilde{w}_2}{\partial \eta} = 0 \quad (\eta = 0), \tag{31b}$$

and analysis of the Ekman extensions at the horizontal boundaries yields

$$\tilde{w}_2 = \tfrac{1}{2}a\delta(\eta), \quad (z = 0, H). \tag{31c}$$

As in other problems, the general solutions can be written as Fourier series, viz.

$$\begin{aligned}\tilde{w}_j &= \sum_{n=1}^{\infty} (a_n\phi_1 + b_n\phi_2 + c_n\phi_3) \sin \frac{n\pi z}{H}, \\ \tilde{v}_j &= -\sum_{n=1}^{\infty} (a_n\phi_1 + b_n\phi_2 - c_n\phi_3) \cos \frac{n\pi z}{H},\end{aligned} \tag{32}$$

with $\phi_1$, $\phi_2$, $\phi_3$ as before, and applying the boundary conditions (31) yields relations from which the coefficients $a_n$, $b_n$ and $c_n$ can be found. Once $\tilde{v}_j$ is determined, $\tilde{u}_j$ follows immediately from (18). For the $j = 2$ field this results in

$$\begin{aligned}\tilde{w}_2(\eta, z) &= \sum_{n=1}^{\infty} D_n\left(\phi_1 + \phi_2\sqrt{3}\right) \sin \frac{n\pi z}{H}, \\ \tilde{v}_2(\eta, z) &= -\sum_{n=1}^{\infty} D_n\left(\phi_1 + \phi_2\sqrt{3}\right) \cos \frac{n\pi z}{H}, \\ \tilde{u}_2(\eta, z) &= -\frac{1}{2}\sum_{n=1}^{\infty} D_n\gamma_n^2\left(\phi_1 - \phi_2\sqrt{3}\right) \cos \frac{n\pi z}{H},\end{aligned} \tag{33}$$

where

$$D_n = \frac{a}{H\sqrt{3}} \frac{1-(-1)^n}{\gamma_n^2}.$$

It can be verified by integrating $\tilde{w}_2$ with respect to $\eta$ that this field produces a vertical $O(E^{1/2})$ flux

$$\int_0^{\infty} \tilde{w}_2(\eta, z)\, d\eta = \tfrac{1}{4}a, \tag{34}$$

which is exactly the required magnitude. This completes the analysis of the $O(E^{1/2})$ circulation in the fluid film.

## 4. The thin-film case: merging Stewartson layers

When the film thickness is decreased to a small value, the geostrophic interior region vanishes, and the Stewartson layers at $r = a$ and $r = b$ will merge. In this section attention is focussed on the situation of a film thickness of the same order as the $E^{1/4}$-layer thickness, i.e. $(b-a) \sim E^{1/4} (> E^{1/3})$. This implies that the film is entirely occupied by the $E^{1/4}$ layer, and, although the $E^{1/3}$ layers will merge, it is assumed that their structure is not affected by the proximity of the boundaries. For a thick film, i.e. $(b-a) > E^{1/4}$, the azimuthal velocity in the $E^{1/4}$ layer is to $O(E^{1/4})$ given by equations (9a) and (14a), and tends to the interior swirl velocity as $\xi \to -\infty$. When the film has a small thickness $(b-a) \sim E^{1/4}$ the $E^{1/4}$ layer no longer shows a transition to a solid-body rotation (due

to the non-existence of the geostrophic interior), and induces a nonvanishing shear stress at the free surface:

$$\left.\frac{\partial V}{\partial r}\right|_{r=a} = E^{-1/4}\left.\frac{\partial V^{(0)}}{\partial \xi}\right|_{\xi_a} + \left.\frac{\partial V^{(1)}}{\partial \xi}\right|_{\xi_a} + \mathrm{O}(E^{1/4}), \tag{35}$$

with $\xi_a = \xi(r=a) = (a-b)E^{-1/4}$. To leading order, i.e. to $\mathrm{O}(E^{-1/4})$, substitution of (9a) and (14a) yields

$$\left.\frac{\partial V}{\partial r}\right|_{r=a} = -\tfrac{1}{2}sbE^{-1/4}\exp(s\xi_a). \tag{36}$$

This obviously requires a correction by an $E^{1/4}$ layer at the free surface, as this surface must be free of any stresses. A similar situation has been examined in a recent paper by Ungarish and Greenspan [14]. The $E^{1/4}$ layer at $r=a$ is also governed by the equations (6)-(8), now with $\xi^* = (r-a)E^{-1/4}$ as the radial coordinate. Equation (8) has the following non-divergent solution for the correction azimuthal velocity:

$$V^*(\xi^*) = A + B\exp(-s\xi^*), \tag{37}$$

in which the unknown coefficients can be determined by requiring

$$V^*(\xi^* \to \infty) = 0, \quad \left.\frac{\partial V^*}{\partial \xi^*}\right|_{\xi^*=0} = \tfrac{1}{2}sb\exp(s\xi_a), \tag{38}$$

yielding

$$A = 0, \quad B = -\tfrac{1}{2}b\exp(s\xi_a). \tag{39}$$

From these results it is obvious that the correction velocity vanishes as $\xi_a \to -\infty$. Associated with the azimuthal velocity, there is also a vertical correction velocity,

$$W^*(\xi^*, z) = -Bs\left(\frac{1}{2} - \frac{z}{H}\right)\exp(-s\xi^*), \tag{40}$$

which is $\mathrm{O}(E^{1/4})$. The vertical $\mathrm{O}(E^{1/2})$ flux produced by this correction field must be counteracted by a correction $j=2$ field in the Stewartson $E^{1/3}$ layer at the free surface. The general (non-divergent) solutions for this correction field are again given by (32), with $\eta$ replaced by $\eta^* = (r-a)E^{-1/3}$, and the coefficients can be found by applying the boundary conditions

$$\frac{\partial \tilde{v}_2^*}{\partial \eta^*} = 0, \quad \frac{\partial \tilde{w}_2^*}{\partial \eta^*} = 0 \quad (\eta = 0), \tag{41a}$$

$$\int_0^\infty \tilde{w}_2^*(\eta^*, z)\,\mathrm{d}\eta^* = \left(\frac{1}{2} - \frac{z}{H}\right)B. \tag{41b}$$

This yields

$$\tilde{w}_2^*(\eta^*, z) = \sum_{n=1}^{\infty} E_n\left(\phi_1 + \phi_2\sqrt{3}\right) \sin \frac{n\pi z}{H},$$
$$\tilde{v}_2^*(\eta^*, z) = -\sum_{n=1}^{\infty} E_n\left(\phi_1 + \phi_2\sqrt{3}\right) \cos \frac{n\pi z}{H} \quad , \tag{42}$$

with

$$E_n = -\frac{B}{\pi\sqrt{3}} \gamma_n \frac{1 + (-1)^n}{n},$$

and $\phi_1$, $\phi_2$ being given by (23).

## 5. Comparison with observations and numerical results

The experimental and numerical work performed by Shadday et al. [1] offers the opportunity to verify the validity of the linear analysis presented in the previous sections. These investigators have carried out accurate velocity measurements in a rotating cylinder of radius $R = bL = 9.45$ cm and height $\bar{H} = HL = 19.43$ cm ($L$ is the scaling parameter). In all experiments the angular speed of the cylinder measured 1000 r.p.m., while the upper endcap had a fixed overspeed of $\epsilon = +5\%$. Results were obtained for two values of the film thickness $(b - a)L$, viz. a thick film of 4.22 cm and a thin film of 1.91 cm, corresponding to inner radii of $aL = 5.23$ cm and 7.54 cm, respectively. The scaling factor is here taken to be $L = 9.45$ cm, so that $b = 1$ and $H = 2.056$. In the terminology of Shadday et al., the Ekman number $E^*$ is defined as $E^* = \nu/(\Omega H^2)$ and measures $2.5 \times 10^{-6}$, which implies that the Ekman number $E$ as introduced in Section 2 has a magnitude of

$$E = \left(\frac{H}{L}\right)^2 E^* = 1.06 \times 10^{-5}. \tag{43}$$

In the so-called *thick-film case* a substantial portion of the fluid is in geostrophic balance, and viscous effects are confined to relatively thin layers at the flow boundaries. Figures 2a and 2b show combined diagrams of the composite analytical velocities in vertical and azimuthal direction:

$$W = E^{2/12}\left(\tilde{w}_{2a} + \tilde{w}_{2b}\right) + E^{3/12}\left(\tilde{w}_{3b} + W_b^{(0)}\right) + E^{6/12}\left(\tilde{w}_{6b} + W_b^{(1)}\right) + \mathrm{O}(E^{7/12}), \tag{44}$$

$$V = v_I + V_b^{(0)} + E^{2/12}\left(\tilde{v}_{2a} + \tilde{v}_{2b}\right) + E^{3/12}\left(\tilde{v}_{3b} + V_b^{(1)}\right) + \mathrm{O}(E^{4/12}), \tag{45}$$

where the subscripts $a$ and $b$ refer to the radius of the boundary which the shear layer is attached to. Also shown are the numerical results taken from Shadday et al. ([1], Figures

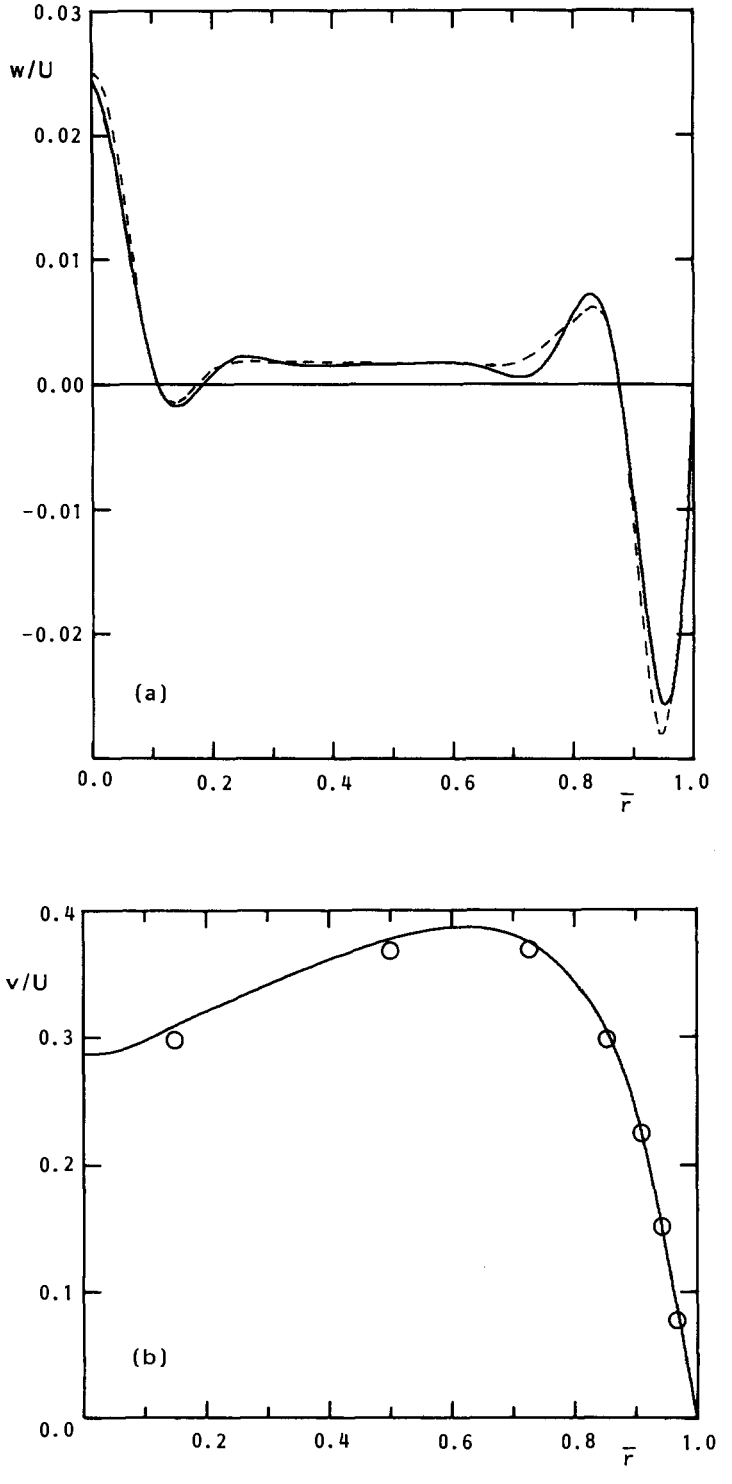


Figure 2. Radial distribution of the axial (a) and the azimuthal (b) velocity at $z = 0.5H$; film thickness = 4.22 cm, $E = 1.06 \times 10^{-5}$, $\epsilon = 0.05$. Analytical profiles are represented by solid lines, while the broken line and the dots represent numerical data obtained by Shadday et al. [1]. Velocities are scaled by the perturbation velocity $U = \epsilon \Omega L$, and the radial position is normalized by the film thickness, i.e. $\bar{r} = (r - a)/(b - a)$.

10 and 11). The radial coordinate is defined as $\bar{r} = (r - a)/(b - a)$, and the velocities are scaled by the imposed perturbation velocity $U = \epsilon\Omega L$. The agreement between the analytical and numerical results is very good. This is remarkable as nonlinear effects have (in contrast with the numerical model) been neglected in the analysis, while the condition $\epsilon < O(E^{1/4})$ for linear flow (cf. Bennetts and Hocking [15]) is not convincingly satisfied in

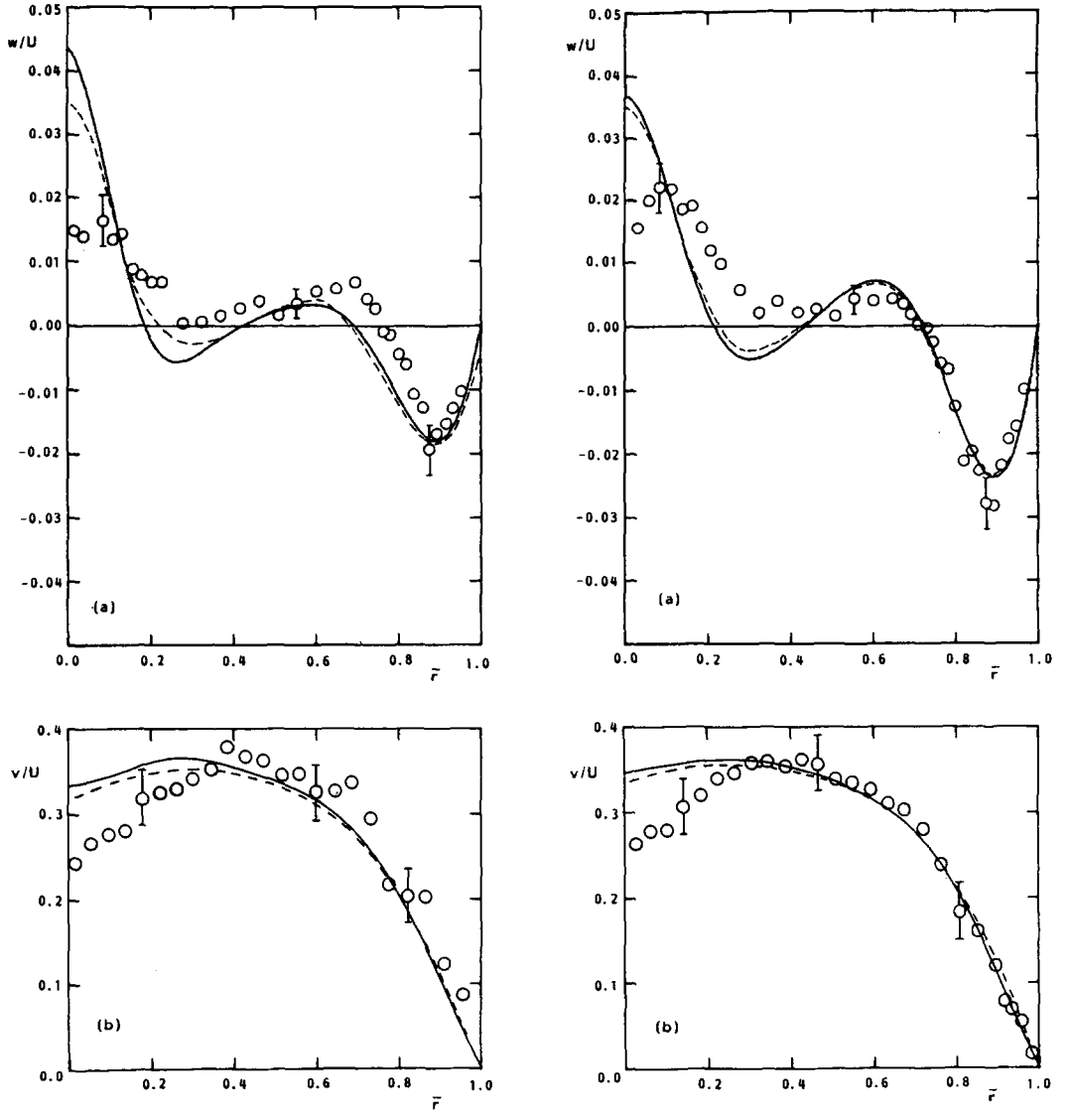


Figure 3. Radial distribution of the axial (a) and azimuthal (b) velocity at $z = 0.242H$; film thickness = 1.9 cm, $E = 1.06 \times 10^{-5}$, $\epsilon = 0.05$. The solid lines represent analytical profiles, while the numerical and experimental data by Shadday et al. [1] are represented by broken lines and by dots, respectively. Velocities and radial position are normalized as in Figure 2.

Figure 4. Radial distribution of the axial (a) and azimuthal (b) velocity at $z = 0.438H$. Same parameter values as in Figure 3.

the configuration considered, since $\epsilon \simeq E^{1/4} \simeq 0.05$. This phenomenon has also been reported by Shadday et al.: they have calculated the flow numerically from both the linear and the nonlinear basic equations, and obtained results that were very similar. It thus seems that weakly nonlinear flows are still governed by linear Stewartson-layer theory.

It can be clearly observed from the velocity distribution shown in Figure 2a that the vertical velocity has a constant low value in the geostrophic interior region, with the largest velocities occurring in the shear layers. The Stewartson layers have typical

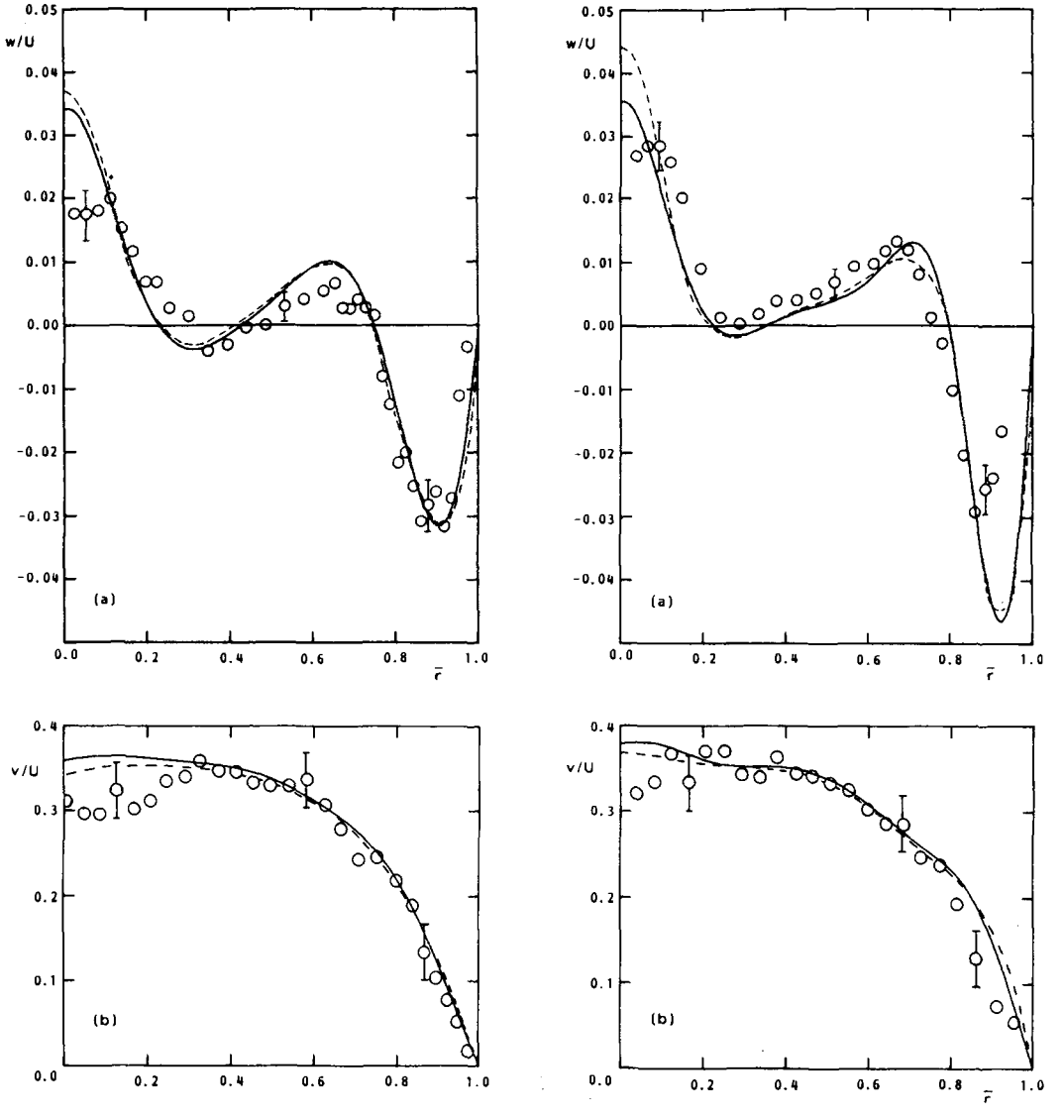


Figure 5. Radial distribution of the axial (a) and azimuthal (b) velocity at $z = 0.634H$. Same parameter values as in Figure 3.

Figure 6. Radial distribution of the axial (a) and azimuthal (b) velocity at $z = 0.83H$. Same parameter values as in Figure 3.

thicknesses $LE^{1/4} = 0.5$ cm and $LE^{1/3} = 0.2$ cm, which are small compared to the film thickness (4.22 cm). It is emphasized that the characteristic boundary-layer thicknesses are mathematically determined by putting $|\xi| = 1$ and $|\eta| = 1$, respectively. In physical situations, however, the shear-layer thickness may appear to exceed the "typical" thickness by a factor of 4 or more. This can be seen in Fig. 2a, where the physical thicknesses of the $E^{1/3}$ layers at $r = a$ and $r = b$ measure 1.25 cm and 0.85 cm, respectively, which both are considerably larger than the above-mentioned typical thickness $LE^{1/3}$.

In the *thin-film case* the Stewartson-layer thicknesses therefore become comparable to the film thickness (1.9 cm), and a distinct boundary between the various flow regions will no longer be visible. It has been pointed out in Section 4 how the solutions presented in Section 3 should be corrected for merging shear layers, in order to ensure that the shear stress at the free surface is zero. Composite velocity profiles for the 'thin-film case' have also been calculated according to (44) and (45), now being extended by the correction velocities (37), (40) and (42). Radial distributions of the axial and azimuthal velocities at the axial positions $z/H = 0.242$, 0.438, 0.634, 0.83 are shown in Figures 3 to 6 which also present the numerical curves and the experimental data obtained by Shadday et al. [1]. In

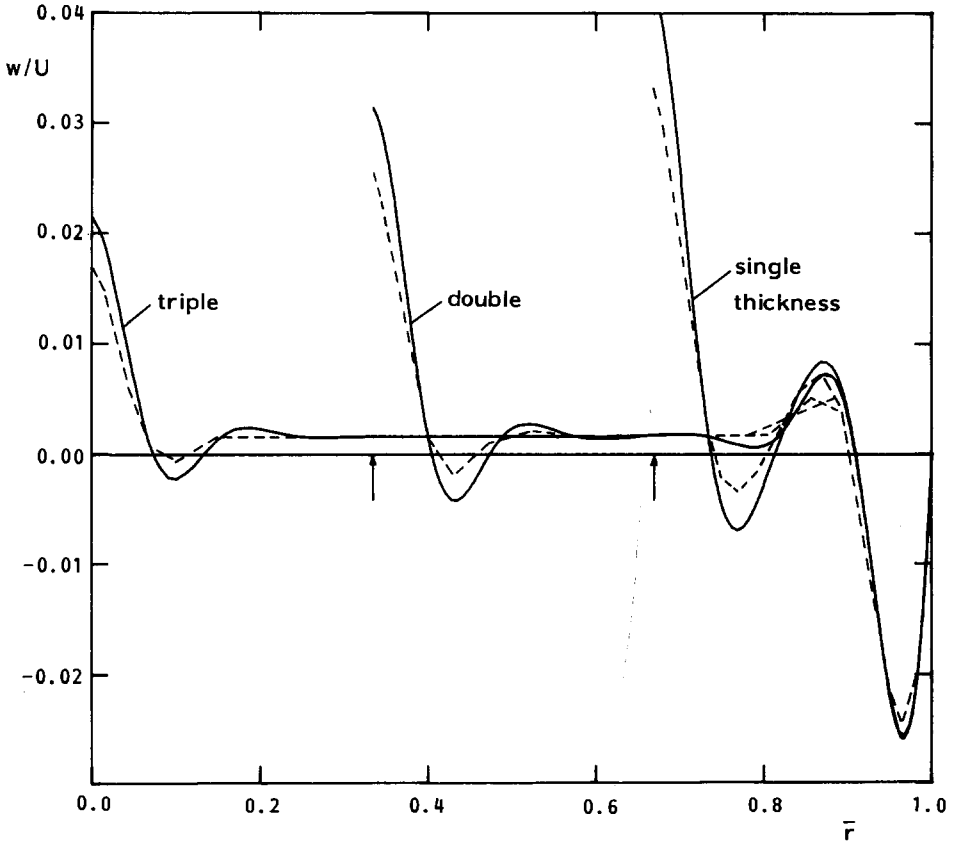


Figure 7. Radial distribution of the axial velocity at $z = 0.5H$ in films of single, double and triple thickness. Parameter values as in Figure 3; the single film thickness measures 1.9 cm. The broken lines represent numerical curves by Ribando and Shadday [16]. Arrows indicate free surface positions of the single and double thickness films.

general the analytically obtained velocity profiles agree well with the numerical curves, both in shape and amplitude. It appears that the discrepancies are largest (though still relatively small) near the free surface $\bar{r} = 0$. The vertical velocity graphs clearly show a smooth merging of the Stewartson $E^{1/3}$ layers, due to the absence of a geostrophic flow region.

Unfortunately, Shadday et al. [1] have not performed any velocity measurements in the thick-film case (Figure 2), so that a comparison between theoretical and experimental results cannot be made for this case. However, experimental velocity profiles are available

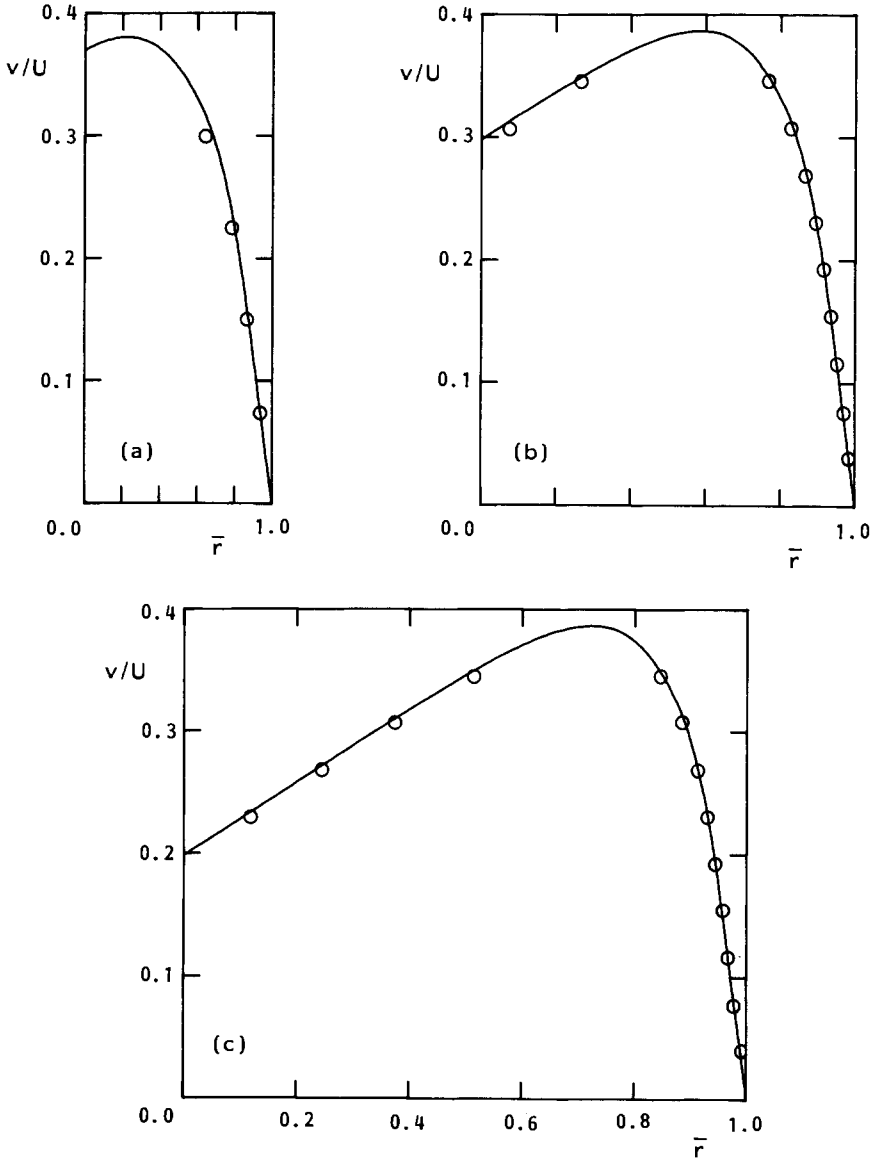


Figure 8. Radial distribution of the azimuthal velocity at $z = 0.5H$ in films of single (a), double (b) and triple (c) thickness. Parameter values as in Figure 3; the single film thickness measures 1.9 cm. Numerical data obtained by Ribando and Shadday [16] are indicated by dots.

for the thin-film case (Figures 3-6), and they show reasonable agreement with the numerical and analytical curves. The largest discrepancy occurs near the free surface, where the observed velocities are systematically smaller than those predicted numerically or analytically. These lower values suggest a nonzero shear stress at the air-fluid interface, but it is hard to explain this discrepancy conclusively without knowing details of the laboratory experiments. Apart from the deviations at the free surface, the observed axial velocity profiles agree fairly well with the theoretical curves, which approximately lie within the range of experimental uncertainty. An exception is seen in Figure 6a, where the serious discrepancy occurs near the sidewall ($r = b$); an explanation is not known. In general though, the qualitative and quantitative agreement between theory and experiment is good, and large discrepancies as measured by Baker [10] in a different shear-layer configuration are only incidental.

Recently, a paper appeared by Ribando and Shadday [16] in which they presented additional numerical results for the partially-filled rotating-cylinder configuration; they now examined the possibility of using analytical expressions for the Ekman conditions instead of grid refinement and application of the no-slip conditions at the horizontal boundaries. Numerical calculations were performed for fluid films of single, double and triple thickness, the single thickness again being 1.9 cm. For completeness those results are also compared with the present analytical velocity profiles, see Figures 7 and 8. Again, the agreement between theoretical and numerical curves is excellent, once more demonstrating the validity of the linearized analytical description of this weakly nonlinear flow situation.

## References


[1] M.A. Shadday, R.J. Ribando and J.J. Kauzlarich, Flow of an incompressible fluid in a partially filled, rapidly rotating cylinder with a diffentially rotating endcap, *J. Fluid Mech.* 130 (1983) 203–218.

[2] J.A. Johnson, Source-sink flow in a rotating fluid, *Proc. Camb. Phil. Soc.* 75 (1974) 269–282.

[3] A.T. Conlisk and J.D.A. Walker, Incompressible source-sink flow in a rapidly rotating contained annulus, *Q.J. Mech. Appl. Math.* 34 (1981) 89–109.

[4] A.T. Conlisk and J.D.A. Walker, Forced convection in a rapidly rotating annulus, *J. Fluid Mech.* 122 (1982) 91–108.

[5] G.J.F. van Heijst, The shear-layer structure in a rotating fluid near a differentially rotating sidewall, *J. Fluid Mech.* 130 (1983) 1–12.

[6] K. Stewartson, On almost rigid rotations, *J. Fluid Mech.* 3 (1957) 17–26.

[7] D.W. Moore and P.G. Saffman, The structure of free vertical shear layers in a rotating fluid and the motion produced by a slowly rising body, *Phil. Trans. R. Soc.* A264 (1969) 597–634.

[8] K. Hashimoto, A source-sink flow of an incompressible rotating fluid, *J. Phys. Soc. Japan* 38 (1975) 1508–1515.

[9] D.J. Baker, A technique for the precise measurement of small fluid velocities, *J. Fluid Mech.* 26 (1966) 573–575.

[10] D.J. Baker, Shear layers in a rotating fluid, *J. Fluid Mech.* 29 (1967) 165–175.

[11] L.P. Cook and G.S.S. Ludford, Higher-order approximation for free shear layers in almost rigid rotations, *J. Fluid Mech.* 69 (1975) 191–195.

[12] G.P. Tolstov, *Fourier series*, Dover Publications, New York (1962).

[13] G.J.F. van Heijst, Source-sink flow in a rotating cylinder, *J. Engng. Math.* 18 (1984) 247–257.

[14] M. Ungarish and H.P. Greenspan, On the radial filling of a rotating cylinder, *J. Fluid Mech.* 141 (1984) 97–107.

[15] D.A. Bennetts and L.M. Hocking, On nonlinear Ekman and Stewartson layers in a rotating fluid, *Proc. R. Soc. Lond.* A333 (1973) 469–489.

[16] R.J. Ribando and M.A. Shadday, The Ekman matching condition in a partially filled, rapidly rotating cylinder, *J. Comp. Phys.* 53 (1984) 266–288.